Journal Pre-proof

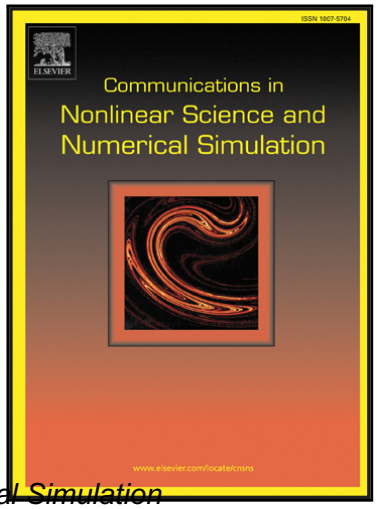

A flight formation mechanism: the weight of repulsive force

Jian Gao, Changgui Gu, Huijie Yang, Man Wang

PII: S1007-5704(20)30478-0
DOI: https://doi.org/10.1016/j.cnsns.2020.105648
Reference: CNSNS 105648

To appear in: *Communications in Nonlinear Science and Numerical Simulation*

Received date: 14 April 2020
Revised date: 28 August 2020
Accepted date: 29 November 2020

Please cite this article as: Jian Gao, Changgui Gu, Huijie Yang, Man Wang, A flight formation mechanism: the weight of repulsive force, *Communications in Nonlinear Science and Numerical Simulation* (2020), doi: https://doi.org/10.1016/j.cnsns.2020.105648

Highlights

- Improved the Boid model to describe migrating bird flocks.
- Explained the formation mechanism of flight formations of birds from a new perspective.
- Explained the reasons for the differences between flight formations of large and small birds.
- Single-row flight formation has higher migration speeds.
- Theoretically found several different flight patterns of bird flocks.

A flight formation mechanism: the weight of repulsive force

Jian Gao[a], Changgui Gu[a,*], Huijie Yang[a], Man Wang[b]

[a] *University of Shanghai for Science and Technology, Shanghai 200093, P. R. China*
[b] *Qingdao University, Qingdao 266071, P. R. China*

Abstract

Large birds always choose orderly flight formations for migration. The energy-saving hypothesis and visual communication hypothesis have provided explanations for the formation mechanisms of flight formations of large birds. However, the experimental data differ greatly from the theoretical results of the energy-saving hypothesis, and the visual communication hypothesis lacks sufficient supporting evidence. Moreover, neither of these two hypothesises can explain the differences between flight formations of large and small birds. In this article, the authors investigated the formation mechanism of bird flocks from a new perspective, i.e., the weight of repulsive force between individuals, and provided explanations for the differences between flight formations of large and small birds. The authors believe that the weight of repulsive force between large birds is greater than that between small birds, which makes them better at preventing collisions between individuals. The simulation results show that as the weight of repulsive force between individuals is gradually increased, the flight formation of the flock converts from a cluster formation (corresponding to the flight formation of small birds) to a single-row formation (corresponding to the flight formation of large birds). And the migration speed of the single-row flight formation is larger than that of the cluster formation. In addition, the authors also studied the effects of population and density of individuals on flight formations: the entire flock will lose the ability to migrate when the number or density of individuals is large enough. The findings of this article may provide theoretical guidance for the autonomous control for unmanned aerial vehicle swarms.

Keywords: collective behavior; self-organization; animal groups; multi-agent; migratory birds

1. Introduction

An ordered linear formation of migrating flamingos, pelicans, cormorants, cranes, geese, swans, or other large birds is a spectacular phenomenon that gives rise to interesting questions [1]. Yet, most small birds that migrate in flocks always do so in less ordered groups [2, 3, 4]. Why there is such a big difference in flight formation between large and small birds? What is the advantage of the ordered linear formation (see Movie S1), and why do mainly large birds use this type formation? Two hypotheses, i.e., the visual communication and energy saving hypotheses, have attempted to explain such formations to date [1, 2, 5].

The visual communication hypothesis believes that the ordered linear flight formation may enhance communication and orientation of the flock [1, 5, 6]. The two most important things for birds' long-distance flights are information exchange and avoiding the attack of predators. The flock uses an ordered linear formation when flying so that each bird can see the entire flock, and they can better adjust their position in the formation, avoid collisions, and communicate. At the same time, flight formation is conducive to jointly defending the attack of predators and improving the overall survival probability. Therefore, each bird can obtain the overall experience information of the flock and achieve higher group cooperation efficiency. This hypothesis seems very reasonable, but lacks effective evidence to support it [1]. Alternatively, the energy saving hypothesis believes that during the flight formation, when an individual flaps its wings, its tail will cause a swirling airflow. If its neighbour behind it is right in the vortex's updraft, the individual will save a lot of physical strength and then can fly longer distances [7]. This hypothesis was first proposed by the

*Corresponding author
Email address: gu_changgui@163.com (Changgui Gu)

German aerodynamicist Wieselsberger (see Ref. [7]). Since then, Lissaman [8] used the aerodynamic theory to make a simulated estimate of formation flight. Specifically, in a downwind condition, a cooperative flock flight consisting of 25 individuals will increase the flight distance by about 70% compared to when the individuals fly alone, and the best effort-saving angle of the formation is 120°. However, in their estimation simulations, no specific calculation formula was given, and no detailed calculation process was provided. Instead, a simple model is used, assuming that the wings of these individuals are the same as the wings of the aircraft, regardless of the essential difference between these two. Unfortunately, subsequent studies have shown that the energy saving rate of flight formation is much smaller than Lissaman's simulation estimate [8]. Subsequent researchers expounded the principle and function of the vortex airflow in formation flight from the perspective of geometry and dynamics, and analyzed and verified the formation energy saving hypothesis in detail [9, 10, 11, 12]. For instance, Andersson [1] verified the hypothesis of formation effort through actual observation methods. Weimerskirch [13] showed that great white pelicans (Pelecanus onocrotalus) have lower heart and wing beat rates, glide more often than other birds, and save as much as 11-14% energy when flying in the vortex wake from another bird. In summary, although the both two hypotheses above explain the formation mechanism, they are quite different from the real situations. Consequently, the research on the formation of bird flocks is still in the exploration and research stage.

Flight formations of flocks always exhibit similar behaviors regardless of the differences between species and individual sizes. Accordingly, there should be a general principle governing collective behaviors of bird flocks. To model individuals, abstracted as particles that are self-propelled and interactive (making their motions consistent with their neighbors), has been one way to reveal these principles [14, 15, 16, 17, 18, 19]. In addition to local velocity (the velocity of a certain particle), some models involve attractive and repulsive (social) forces between particles [20]. For instance, Ref. [3] studies the unique flight formation of starlings by modeling, and suggests that the flock is in a critical state, making the entire flock ready to respond maximally and significantly to external disturbances at any moment. Ref. [21] studies the cooperative behavior of ants through modeling. Ref. [22] explained the simultaneous turning of pigeons. Even, Refs. [23, 24, 25] studies the collective behavior of human being. Therefore, the modeling method can be an effective measure to reveal the inherent mechanisms of collective behaviors.

Understanding and mastering the formation mechanism of bird flock flight formation can provide theoretical guidance for the autonomous control for unmanned aerial vehicle (UAV) swarms [26, 27]. With the deepening application of unmanned and autonomous technology, the development of UAV swarm autonomous system has become an important field of UAV research, because through close cooperation, the UAV swarm autonomous system can show better coordination, intelligence and autonomous capability than the artificial system [28]. Increasingly complex missions and environments constantly challenge the autonomy of UAV systems [29, 30].

In this study, we investigated the formation mechanism of bird flocks from a new perspective, and provided explanations for the differences between flight formations of large and small birds. We also studied the effects of population and density of individuals on flight formations. The rest of this study is organised as follows. Section 2 introduces the method and model; in Section 3 the numerical results are presented; and then, Section 4 shows the analytical results; at last, conclusion are presented in Section 5.

2. Method

To explain the difference between the flight formations of large and small birds, i.e., large birds are generally organized in a row, and small birds often have irregular flight formations, we believe that this difference in flight formations should be related to the size of the birds. Large birds have a larger mass than small birds, resulting in greater inertia when flying (suppose the velocity of flight is constant). Because the impact force caused by the collision of objects is positively related to the mass of the object, large birds will take more damage if they collided with others. Therefore, large birds would pay more attention to preventing collisions with other individuals. Consequently, we propose a hypothesis that the difference in flight formations of large and small birds is partially due to the different weights of repulsive forces between individuals. Specifically, large birds give greater weight to repulsion between individuals to prevent collisions. In the following, we modify the Boid model [15, 35] to perform numerical simulations.

2.1. Rules of behavior

- Within a certain range around each individual, there is a social force reducing the distance between individuals, called the attractive force, between individuals, which increases with the increase of distance;

- All individuals in the same region tend to fly in a same direction, i.e., individuals are subject to a social force, called the polarization force, that makes the flight direction consistent;
- Each individual attempts to keep a certain distance from others at all times. Thus, within a certain range around each individual, there is a social force increasing the distance between individuals, called the repulsive force, between individuals, which increases with the decrease of distance;
- The isolated individuals are attracted by the closer neighbors to avoid being isolated, i.e., isolated individuals are affected by a type of social force, called the anti-isolated force;
- In order to ensure the migration of bird flocks, all individuals are subject to a long-distance social force, called the migration force, whose direction is the migration direction. Because bird flocks are more likely to be influenced by the forces between individuals (the attractive force, polarization force, repulsive force and anti-isolated force) when they form teams, the migration force should be much weaker than other forces;
- Speeds of individuals cannot exceed a certain upper limit.

2.2. *Model building*

N individuals ($i = 1,2,3,\ldots,N$) with position vectors $\vec{p}_{i,t}$, are simulated in a continuous two-dimensional space, where t indicates the time. Because the response speeds of animals are limited, time is partitioned into discrete time steps in the model, and velocity vectors $\vec{v}_{i,t}$ indicate the increment of $\vec{p}_{i,t}$ in each time step. The position of each individual at time $t+1$ can be expressed as

$$\begin{aligned} \vec{p}_{i,t+1} &= \vec{p}_{i,t} + \vec{v}_{i,t}, \\ \vec{v}_{i,t+1} &= \frac{\vec{v}_{i,t} + \vec{F}_{i,t}}{|\,\vec{v}_{i,t} + \vec{F}_{i,t}\,|} v_{max}, \\ i &= 1,2,3,\ldots,N. \end{aligned} \tag{1}$$

Moreover, the change of velocity direction $\delta\theta$ is affected by Gaussian white noise, i.e.,

$$\theta_{i,t+1} = \theta_{i,t} + \delta\theta_{i,t} + \sigma W_G, \tag{2}$$

where W_G indicates Gaussian white noise with variance of 1 and the mean value of 0, and σ is noise intensity. $\theta_{i,t}$ indicates the direction angle of individual i at time t, and the $\delta\theta_{i,t}$ indicates the change of direction angle of individual i at time t. In Eq. (1), $\vec{F}_{i,t}$ indicates the resultant force of all social forces acting on the individual i at time t, and v_{max} is the maximum speed that an individual can reach. Specifically,

$$\vec{F}_{i,t} = w_0\vec{f} + w_1\vec{F}'_{i,t} + w_2\vec{F}''_{i,t} + w_3\vec{F}'''_{i,t} + w_4\vec{f}'_{i,t}, \tag{3}$$

where $\vec{f}$, $\vec{F}'_{i,t}$, $\vec{F}''_{i,t}$, $\vec{F}'''_{i,t}$ and $\vec{f}'_{i,t}$ indicate the migration force, attractive force, polarization force, repulsive force and the anti-isolation force, respectively. w_0, w_1, w_2, w_3 and w_4 are parameters (weighting parameters) that control the weight of each type of forces. The forces are calculated as follows. $n_{i,t,1}$ is the total number of other individuals in the circular region with the individual i as the center and r_1 as the radius. $\vec{P}_{i,t}$ is the center of gravity of all other individuals in the region, i.e.,

$$\vec{P}_{i,t} = \sum_{j=1}^{n_{i,t,1}} \frac{\vec{p}_{j,t}}{n_{i,t,1}}, \tag{4}$$

where $\vec{p}_{j,t}$ indicates the position vector of each neighbour of the individual i in the region. The attractive force acting on the individual i at time t can be expressed as

$$\vec{F}'_{i,t} = \vec{P}_{i,t} - \vec{p}_{i,t}. \tag{5}$$

The polarization force acting on the individual i at time t is expressed as

$$\vec{F}''_{i,t} = \sum_{j=1}^{n_{i,t,1}} \frac{\vec{v}_{j,t}}{n_{i,t,1}}, \tag{6}$$

where $\vec{v}_{j,t}$ indicates the velocity vector of each neighbour of the individual i in this region. Each individual would attempt to maintain a minimum distance r_2 ($r_2 < r_1$) from others preventing collisions with other individuals. Consequently, there is a circular region, with the individual i as the center and r_2 as the radius, around each individual i that does not allow other individuals to enter. $n_{i,t,2}$ is the total number of other individuals in the circular region, and $\vec{C}_{i,t}$ is the center of gravity of all other individuals in the region, i.e.,

$$\vec{C}_{i,t} = \sum_{j=1}^{n_{i,t,2}} \frac{\vec{p}_{j,t}}{n_{i,t,2}}, \tag{7}$$

where $\vec{p}_{j,t}$ indicates the position vector of each neighbour of the individual i in this region. The repulsive force acting on the individual i at time t is expressed as

$$\vec{F}'''_{i,t} = \frac{\vec{p}_{i,t} - \vec{C}_{i,t}}{|\vec{p}_{i,t} - \vec{C}_{i,t}|^2}. \tag{8}$$

When the individual i is isolated, it will be affected by the anti-isolation force, i.e.,

$$\vec{f}'_{i,t} = \vec{P}'_{i,t} - \vec{p}_{i,t}, \tag{9}$$

where $\vec{P}'_{i,t}$ is the center of gravity of n' ($n' = 3$) nearest neighbors of the isolated individual i at time t, i.e.,

$$\vec{P}'_{i,t} = \sum_{j=1}^{n'} \frac{\vec{p}_{j,t}}{n'}, \tag{10}$$

where $\vec{p}_{j,t}$ indicates the position vector of n' nearest neighbors of the isolated individual i at time t. The long-distance migration force $\vec{f}$ acting on the individual i is constant. Moreover, consider the following special cases

$$\begin{aligned} \vec{F}'_{i,t} &= 0, \quad if\ n_{i,t,1} = 0, \\ \vec{F}'''_{i,t} &= 0, \quad if\ n_{i,t,2} = 0, \\ \vec{f}'_{i,t} &= 0, \quad if\ n_{i,t,1} \neq 0. \end{aligned} \tag{11}$$

The center of gravity of the group ($\vec{P}^*_t$, Eq (12)) is used to describe the position of the group,

$$\vec{P}^*_t = \sum_{i=1}^{N} \frac{\vec{p}_{i,t}}{N}, \tag{12}$$

The component of the velocity of $\vec{P}^*_t$ in the direction of migration is used to describe the speed of the group's migration, i.e., the migration velocity rate

$$V^*_t = \frac{|\vec{V}_t \cos(\theta^*)|}{v_{max}}, \tag{13}$$

where $\vec{V}_t$ is the velocity of $\vec{P}^*_t$, and θ^* is the angle between the direction of V_t and the direction of migration. Group polarization ($\vec{Q}^*_t$, $0 \leq \vec{Q}^*_t \leq 1$, Eq (14)) is used to measure the degree of alignment among individuals within the group,

$$Q^*_t = \frac{1}{N} \left| \sum_{i=1}^{N} \frac{\vec{v}_{i,t}}{|\vec{v}_{i,t}|} \right|. \tag{14}$$

Table 1: Parameter values for the model.

Parameter	Value	Parameter	Value
v_{max}	0.2	σ	0.01
w_0	0.2	w_1	0.5
w_2	5.0	w_4	1.0
$\lvert\vec{f}\rvert$	0.05	r_1	1.5
r_2	0.3	n'	3

In all simulations, suppose that the initial positions of all individuals are randomly distributed in a rectangular area G, that is,

$$\vec{p}_{i,t_0} \sim U(G), \quad i = 1,2,3,\ldots,N, \tag{15}$$

where G represents a rectangular region with an area of $S_G = N/\rho$, and ρ indicates the average density of the spatial distribution of the birds. The initial direction of all individuals points to a common direction, i.e. the direction to be migrated (specified as horizontal right in this paper). All individuals take off at one certain time, and self-organize the formation in the air.

Various values of the parameter w_3 in the interval $[0.0, 1.0]$ were considered, and the effects of the total number of individuals N and the average density ρ on the migration pattern were both studied, while the other parameters were fixed, which are given in Table 1. The dynamic behaviors of bird flocks was simulated in a two-dimensional unbounded space through Fortran and MATLAB codes, which are available from the authors on request.

3. Numerical results

3.1. Effect of the weighting parameter w_3 on the formation of flocks

We have studied the effects of the weighting parameter w_3 on the collective behavior when the total number N and the average density ρ are both constant ($N = 20$, $\rho = 5$). When the weighting parameter w_3 is equal to 0.01, the formation of the bird flocks can reach a stable state after a period of time (see Movie S2). That is, the relative position between individuals will no longer change (Fig. 1A). But the velocity direction of the bird flock in final states is generally not the direction of migration. Interestingly, the final flight direction of the flock is very sensitive to the initial conditions (random distribution of individuals), i.e., different initial conditions lead to different results. Sometimes one can even observe flocks that are flying in the opposite direction of the migration (see Movie S3). Then the weighting parameter w_3 is gradually increased with a step size of 0.01 to study the effect of w_3 on the formation of bird flocks. When the parameter w_3 is greater than or equal to 0.02, the collective behavior changes. For example, when the parameter w_3 is equal to 0.02, the flock cannot reach a stable state and constantly changes the direction of flight (see Movie S4), but the overall shape of the flock is about a triangle. That is, the head is narrow and the tail is wide (Fig. 1B). As the parameter w_3 continues to increase, the average distance between individuals will increase, resulting in an increased size of the flock. For example, when the parameter w_3 is equal to 0.05, the collective behavior exhibits a dynamic behavior similar to that when the parameter w_3 is equal to 0.02 (see Movie S5), but the size of the flock increases significantly (Fig. 1C). When w_3 is greater than or equal to 0.10, the collective behavior changes. For example, when w_3 is equal to 0.10, the shape of the flock is not an simple triangle, but changes periodically. Specifically, the length of the flock is gradually extended, and then suddenly the shape of the flock changes back to the original triangle. Moreover, the flock's flight direction changes around the direction of migration (see Movie S6). As w_3 continues to increase, the flock will be pulled longer. For example, when w_3 is equal to 0.30, the shape of the flock is gradually extended from the original triangular shape, and sometimes can even form a single-row formation which lasts for a short period of time, and then the flock suddenly changes back to the original triangular shape (see Movie S7). When w_3 is greater than or equal to 0.34, the collective behavior changes again. For example, when w_3 is equal to 0.35, the flock is quickly organized into a stable single-line flock with a flight direction pointing to the migration direction (Fig. 1D, also see Movie S8).

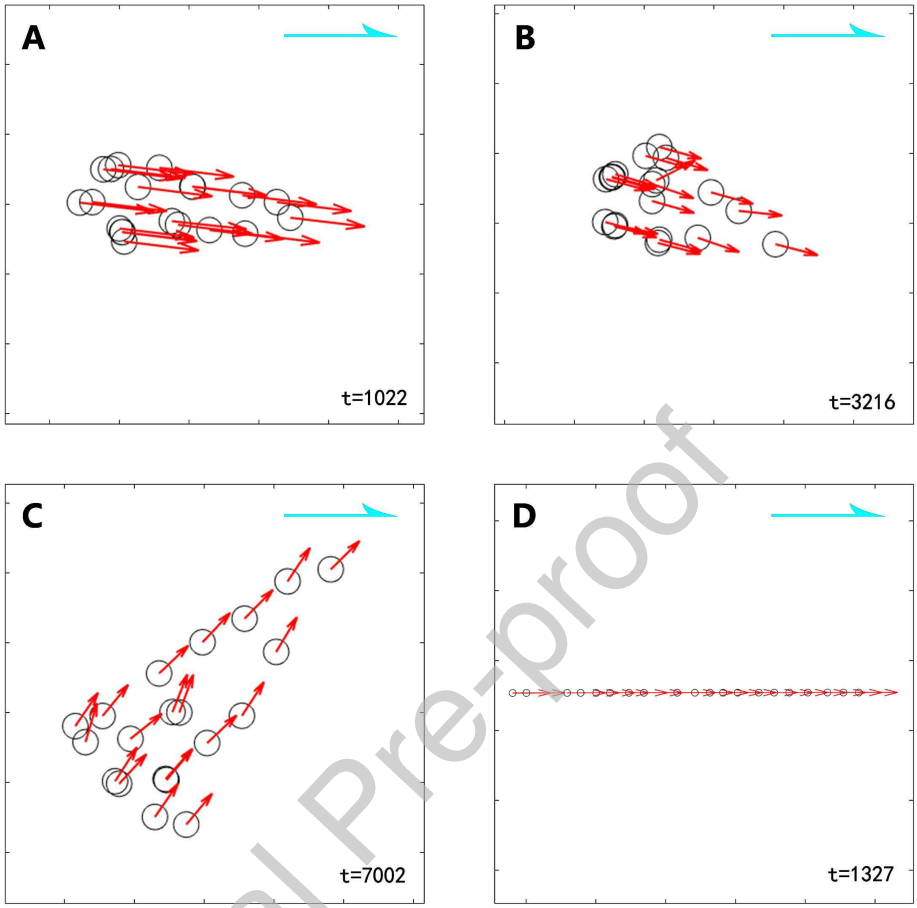

Figure 1: (Color online) The snapshots of collective behaviours exhibited by the model with different parameter w_3: (A) $w_3 = 0.01$, (B) $w_3 = 0.02$, (C) $w_3 = 0.05$ and (D) $w_3 = 0.35$. Horizons of Figures (A), (B) and (C) are 3×3, and the horizon of Figure (D) is 12×12. Black circles and red arrows indicate positions and flight directions of individuals, respectively. The cyan arrow in the upper right corner of each picture indicates the migration direction.

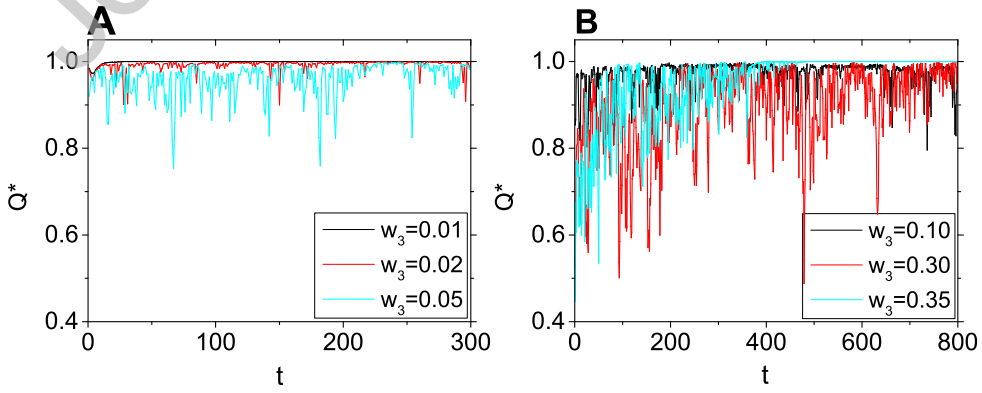

Figure 2: (Color online) Group polarization Q_t^* as a function of t with different weighting parameters w_3.

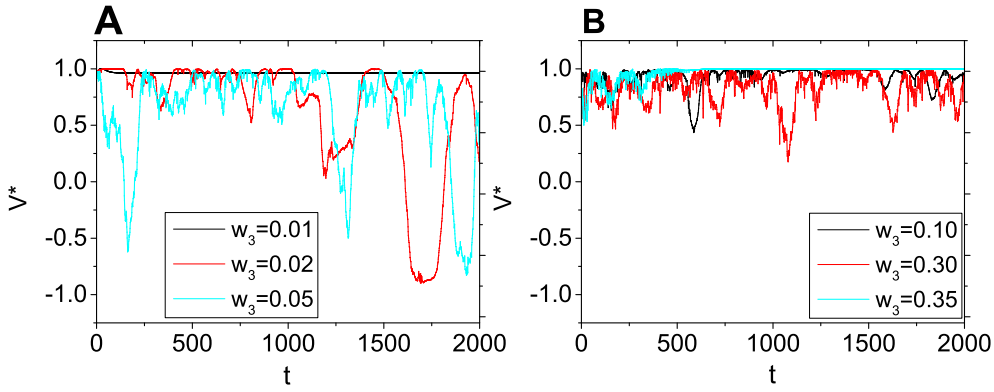

Figure 3: (Color online) Migration velocity rate V_t^* as a function of t with different weighting parameters w_3.

In order to clearly describe the change of the group polarization Q_t^* over time, Q_t^* is plotted as a function of time in Fig. 2. When the weighting parameter w_3 is equal to 0.01, the group polarization Q_t^* quickly (about $t = 30$) increases to 1 and stabilizes at 1, which means that the directions of the individuals in the bird flock quickly become the same, i.e., the directions of each individual point to the same direction. When w_3 is equal to 0.02, Q_t^* cannot be stable at 1, and oscillates near 1. Noted that although Q_t^* is constantly oscillating, its value is always greater than 0.9. It means that although the direction of the individuals in the flock cannot be consistent, the flock maintains a high order. When w_3 increases to 0.05, the oscillation range of Q_t^* increases, but remains above 0.75. When w_3 increases to 0.10, the oscillation range of Q_t^* is similar to the oscillation range when w_3 is equal to 0.05. When w_3 is increased to 0.30, the oscillation range of Q_t^* is larger, and even less than 0.5. It shows that the increase of w_3 will reduce the degree of order of the population. When w_3 increases to 0.35, Q_t^* will stabilize at 1 after a period of oscillation, i.e., the population reaches the highest degree of order.

To measure the speed of migration, the migration velocity rate V_t^* is plotted as a function of time in Fig. 3. When the weighting parameter w_3 is equal to 0.01, the migration velocity rate V_t^* of the flock quickly stabilizes, but it is not equal to 1, indicating that the flock is not flying in the direction of migration. When the weighting parameter w_3 is equal to 0.02, the migration velocity rate V_t^* of the flock can be less than 0 for a long time, indicating that the flock flies in a direction opposite to the migration direction for a long time (negative migration). When w_3 is equal to 0.05, there will be a short period of negative migration in the flock. When w_3 is equal to 0.10 or 0.30, the flocks will not show negative migration, and the migration velocity rate V_t^* remains above 0.5. When w_3 equals 0.35, the migration velocity rate V_t^* of the flock quickly increases to 1, indicating that the flock flies in the direction of migration.

The above experimental results show that when the weighting parameter w_3 is greater than or equal to 0.34, the flock will evolve into a stable single-line flock. The time elapsed during the evolution is written as t^*. Simulation results show that the time t^* is a function of w_3 (Fig. 4). The time t^* increases with the increase of the weighting parameter w_3. When the weighting parameter w_3 is greater than 0.8, t^* stabilizes at about 200.

3.2. Effects of total number N and average density ρ on the formation of flocks

In order to study the effect of the total number of all individuals, N, on collective behaviors, the average density ρ and w_3 were fixed at 5 and 1.25, respectively. We performed simulation experiments on flocks with different numbers of individuals (Fig. 5). The results show that when N is equal to 100, the flock can form a huge team, called the State-1, to fly in the direction of migration (Fig. 5A, also see Movie S9). Eventually this flock can form a stable single-line team. However, when N is equal to 120, the whole flock is split into two parts: one part is migrating, and the other part is trapped in a circular area, flying chaotically, called the State-2 (Fig. 5B, also see Movie S10). When N is equal to 150, the entire flock is trapped in a circular area, flying chaotically, called the State-3 (Fig. 5C, also see Movie S11). The migration velocity rate V_t^* and the group polarization Q_t^* are both about 0. It means that when the total number of birds exceeds a certain threshold, the flock will not be able to migrate.

To study the effect of the average density ρ of individuals on collective behaviors, the total number N and the parameter w_3 were fixed at 300 and 1.25, respectively. We performed simulation experiments on flocks with different

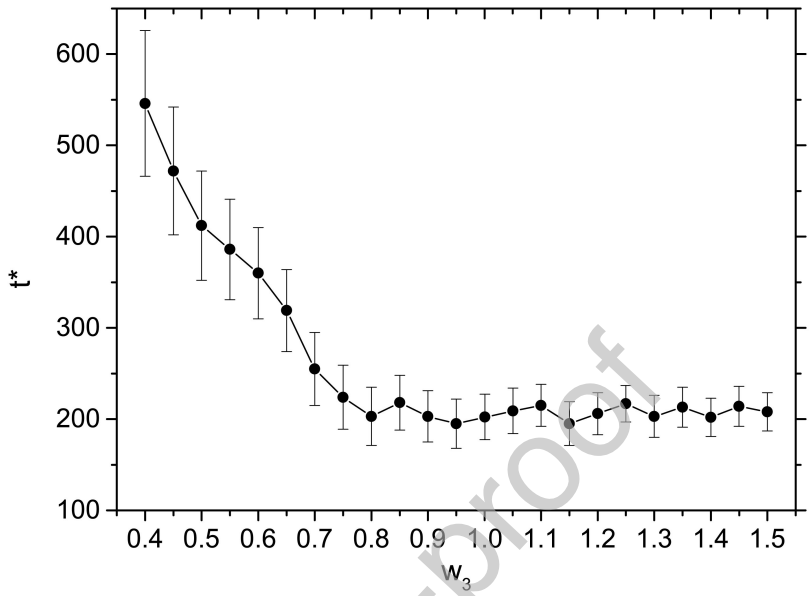

Figure 4: The time t^* as a function of the weighting parameter w_3 with $N = 20$ and $\rho = 5$. As the weighting parameter w_3 increases, the standard deviation of t^* gradually decreases from about 70 to about 20. The data corresponding to each value of the weighting parameter w_3 are obtained by 20 experiments respectively.

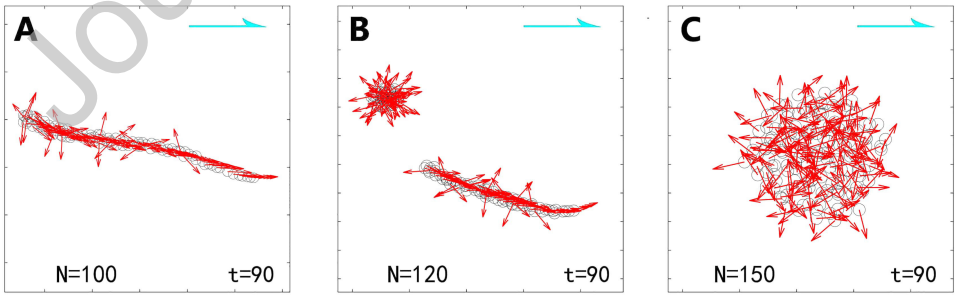

Figure 5: (Color online) The snapshots of collective behaviours exhibited by the model with different total numbers N: (A) $N = 100$, (B) $N = 120$ and (C) $N = 150$. The other parameters are $w_3 = 1.25$ and $\rho = 5$, respectively. The cyan arrow in the upper right corner of each picture indicates the migration direction. Horizons of Figures(A), (B) and (C) are 20×20, 30×30 and 5×5, respectively.

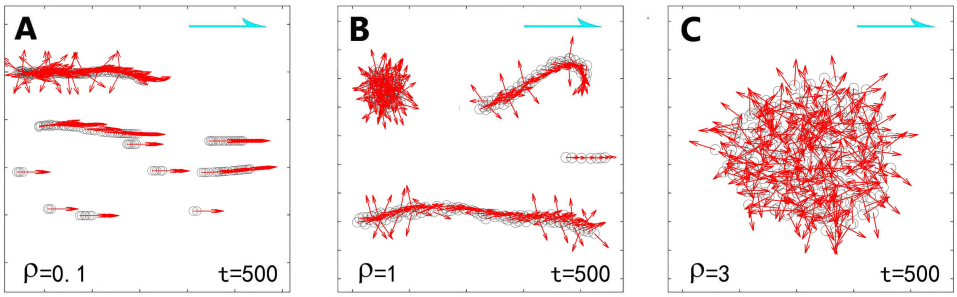

Figure 6: (Color online) The snapshots of collective behaviours exhibited by the model with different total numbers N: (A) $\rho = 0.1$, (B) $\rho = 1$ and (C) $\rho = 3$. The other parameters are $w_3 = 1.25$ and $N = 300$, respectively. The cyan arrow in the upper right corner of each picture indicates the migration direction. Horizons of Figures(A), (B) and (C) are 40×40, 40×40 and 10×10, respectively.

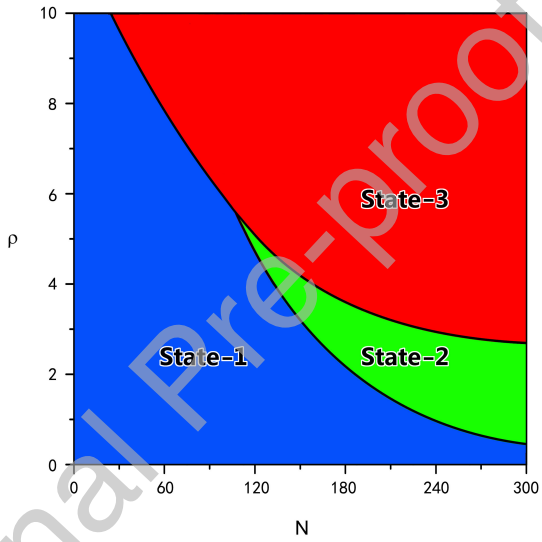

Figure 7: (Color online) Parameter space $(N - \rho)$ for the three types of states. The blue, green and red regions indicates the State-1, State-2 and State-3, respectively.

average density ρ (Fig. 6). The results show that when ρ is equal to 0.1, the flock can form several teams, i.e., the State-1, to fly in the direction of migration (Fig. 6A, also see Movie S12). Eventually, each of these flocks can form a stable single-line team. When ρ is equal to 1, the whole flock is split into two parts: one part is migrating, and the other part is trapped in a circular area, flying chaotically, i.e., the State-2 (Fig. 6B, also see Movie S13). When ρ is equal to 3, the entire flock is trapped in a circular area, flying chaotically, i.e., the State-3 (Fig. 6C, also see Movie S14).

3.3. Parameter space for different states of flocks

In order to obtain the state of the flight formation corresponding to each pair of parameters in the parameter space $(N - \rho)$, where N and ρ are contained in the intervals $(0, 300]$ and $(0, 10]$, respectively, we discretized this parameter space into a 200×200 dot matrix, and tested each pair of parameters (N, ρ) corresponding to each point in the dot matrix to determine the corresponding flight formation state in the parameter space. Figure. 7 shows the distribution of the three states in the parameter space (N, ρ). The smaller N is, the easier it is for flight formations to enter State-1, and the larger ρ is, the easier it is for flight formations to enter State-3. When both N and ρ are smaller, flight formations can only enter State-1. When both N and ρ are larger, flight formations can only enter State-3. In the interval where N

is smaller or ρ is larger, flight formations will not enter State-2. In the interval where N is larger and ρ is smaller, the flight formation is more likely to enter State-2. Overall, the parameter interval supporting State-2 is smaller.

4. Analytical results

In this section, we analyze the occurrence of the flight formations and the causes of phase transition. The simulation results show that the flight formation has two balanced states: one is that the individuals are not on the same straight line (Fig. 1A), and the other is that the individuals are aligned in a straight line (Fig. 1D). It is not difficult to understand that in a balanced formation, the direction of the resultant force acting on each individual is the direction of collective movement, or the resultant force is zero. In the following, we analyze the stability of these two types of flight formations.

To simplify the problem, we only analyze the stability between two individuals, i.e., I_1 and I_2. r indicates the distance between these two individuals. The angles between the connection (of these two individuals) and the flight directions of individuals I_1 and I_2 are α_1 and α_2, $0 \leqslant \alpha_{1,2} \leqslant \pi$, respectively. The resultant force of the attractive and repulsive forces acting on individuals I_1 and I_2 are denoted as $\vec{f}''_{1,t}$ and $\vec{f}''_{2,t}$, respectively ($\vec{f}''_{1,t} = -\vec{f}''_{2,t}$). Let the forces $\vec{f}''_{1,t}$ and $\vec{f}''_{2,t}$ be equal to zero, when r is equal to r', i.e.,

$$\begin{aligned} &|\vec{f}''_{1,t}|, |\vec{f}''_{2,t}| \\ &= |w_1\vec{F}'_{i,t} + w_3\vec{F}'''_{i,t}| \\ &= w_1 r' - \frac{w_3}{r'} \\ &= 0. \end{aligned} \tag{16}$$

One can obtain the value of r', i.e.,

$$r' = \sqrt{\frac{w_3}{w_1}}, \quad (r' \leqslant r_1, r_2). \tag{17}$$

$w_2\vec{F}''_{1,t}$ and $w_2\vec{F}''_{2,t}$ is the polarization force acting on the individuals I_1 and I_2 , i.e.,

$$\vec{F}''_{1,t} = \vec{\upsilon}_{2,t}, \quad \vec{F}''_{2,t} = \vec{\upsilon}_{1,t}. \tag{18}$$

$\vec{F}_{r,1,t}$ (or $\vec{F}_{r,2,t}$) indicates the resultant force of $\vec{f}''_{1,t}$, $w_2\vec{F}''_{1,t}$ and $w_0\vec{f}$ (or $\vec{f}''_{2,t}$, $w_2\vec{F}''_{2,t}$ and $w_0\vec{f}$), which will change the direction of the velocity of the individual I_1 (or I_2). The velocity evolution of these two individuals satisfies the equation

$$\begin{aligned} \vec{\upsilon}_{1,t+1} &= \frac{\vec{\upsilon}_{1,t} + \vec{f}''_{1,t} + w_2\vec{\upsilon}_{2,t} + w_0\vec{f}}{|\vec{\upsilon}_{1,t} + \vec{f}''_{1,t} + w_2\vec{\upsilon}_{2,t} + w_0\vec{f}|}\upsilon_{max}, \\ \vec{\upsilon}_{2,t+1} &= \frac{\vec{\upsilon}_{2,t} + \vec{f}''_{2,t} + w_2\vec{\upsilon}_{1,t} + w_0\vec{f}}{|\vec{\upsilon}_{2,t} + \vec{f}''_{2,t} + w_2\vec{\upsilon}_{1,t} + w_0\vec{f}|}\upsilon_{max}, \\ \vec{f}''_{1,t+1} &= (\delta r - \frac{\vec{\upsilon}_{1,t}\cdot\vec{f}''_{1,t}}{|\vec{f}''_{1,t}|} - \frac{\vec{\upsilon}_{2,t}\cdot\vec{f}''_{2,t}}{|\vec{f}''_{2,t}|})(w_1 + \frac{w_3}{r^2})\frac{\vec{f}''_{1,t}}{|\vec{f}''_{1,t}|}, \\ \vec{f}''_{2,t+1} &= -\vec{f}''_{1,t+1}, \end{aligned} \tag{19}$$

where $\vec{\upsilon}_{1,t}$ and $\vec{\upsilon}_{2,t}$ indicate the velocities of individuals I_1 and I_2, respectively. Specifically, the components in the Cartesian coordinate system can be expressed as

$$\vec{\upsilon}_{1,t} = (\upsilon_{1,x,t},\ \upsilon_{1,y,t})^T, \quad \vec{f}''_{1,t} = (f''_{1,x,t},\ f''_{1,y,t})^T. \tag{20}$$

Eq. (20) has four types of equilibrium solutions, i.e., the Formation 1

$$\begin{aligned} &\upsilon_{1,x} = \upsilon_{max},\ \upsilon_{1,y} = 0, \\ &\upsilon_{2,x} = \upsilon_{max},\ \upsilon_{2,y} = 0, \\ &\vec{f}_1'' = 0,\ \vec{f}_{2,}'' = 0, \end{aligned} \tag{21}$$

the Formation 2

$$\begin{aligned} &\upsilon_{1,x} = -\upsilon_{max},\ \upsilon_{1,y} = 0, \\ &\upsilon_{2,x} = -\upsilon_{max},\ \upsilon_{2,y} = 0, \\ &\vec{f}_1'' = 0,\ \vec{f}_{2,}'' = 0, \end{aligned} \tag{22}$$

the Formation 3

$$\begin{aligned} &\upsilon_{1,x} = \upsilon_{max},\ \upsilon_{1,y} = 0, \\ &\upsilon_{2,x} = \upsilon_{max},\ \upsilon_{2,y} = 0, \\ &f_{1,y}'' = 0,\ f_{2,y}'' = 0, \\ &f_{1,x}'' + w_2\upsilon_{2,x} + w_1 f_x > -\upsilon_{max}, \\ &f_{2,x}'' + w_2\upsilon_{1,x} + w_1 f_x > -\upsilon_{max}, \end{aligned} \tag{23}$$

and the Formation 4

$$\begin{aligned} &\upsilon_{1,x} = -\upsilon_{max},\ \upsilon_{1,y} = 0, \\ &\upsilon_{2,x} = -\upsilon_{max},\ \upsilon_{2,y} = 0, \\ &f_{1,y}'' = 0,\ f_{2,y}'' = 0, \\ &f_{1,x}'' + w_2\upsilon_{2,x} - w_1 f_x < \upsilon_{max}, \\ &f_{2,x}'' + w_2\upsilon_{1,x} - w_1 f_x < \upsilon_{max}. \end{aligned} \tag{24}$$

The Formation 1 (Eq. (21)) and 2 (Eq. (22)) indicate the flight formations when the resultant force of attraction and repulsion acting on each individual is equal to zero. The included angle α_1 can be arbitrary ($0 \leqslant \alpha_1 \leqslant \pi$), and the included angle α_2 is equal to $\pi - \alpha_1$. The former is flying in the direction of migration, while the latter is flying in the opposite direction. Formations 3 (Eq. (23)) and 4 (Eq. (24)) indicate the flight formations when the resultant force of attraction and repulsion acting on each individual is not equal to zero. The connection between the two individuals is parallel to the migration direction, with the former flying in the direction of migration, and the latter in the opposite direction.

Now, we analyze the stability of Formations 1 and 2. Near the equilibrium point, the distance between individuals I_1 and I_2 can be expressed as $r = r' + \delta r$, where δr indicates a small amount. The resultant force of attraction and repulsion acting on both individuals at time t can be approximated, i.e.,

$$\begin{aligned} |\vec{f}_{1,t}''|, |\vec{f}_{2,t}''| &= w_1\vec{F}_{i,t}' + w_3\vec{F}_{i,t}''' \\ &= w_1 r - \frac{w_3}{r} \\ &= w_1(r' + \delta r) - \frac{w_3}{r' + \delta r} \\ &\approx \delta r(w_1 + \frac{w_3}{r'^2}) \\ &= 2\delta r w_1. \end{aligned} \tag{25}$$

To facilitate analysis, when the individual I_1 is on the upper right of individual I_2 in the coordinate system and the small

amount δr is great than zero, Eq. (19) can be transformed into

$$\begin{aligned}
\upsilon_{1,x,t+1} &= \frac{\eta_{1,x}}{\sqrt{\eta_{1,x}^2+\eta_{1,y}^2}}\upsilon_{max},\\
\upsilon_{1,y,t+1} &= \frac{\eta_{1,y}}{\sqrt{\eta_{1,x}^2+\eta_{1,y}^2}}\upsilon_{max},\\
\upsilon_{2,x,t+1} &= \frac{\eta_{2,x}}{\sqrt{\eta_{2,x}^2+\eta_{2,y}^2}}\upsilon_{max},\\
\upsilon_{2,y,t+1} &= \frac{\eta_{2,y}}{\sqrt{\eta_{2,x}^2+\eta_{2,y}^2}}\upsilon_{max},\\
f''_{2,x,t+1} &= f''_{2,x,t}+2w_1(\upsilon_{1,x,t}-\upsilon_{2,x,t}),\\
f''_{2,y,t+1} &= f''_{2,y,t}+2w_1(\upsilon_{1,y,t}-\upsilon_{2,y,t}),
\end{aligned} \tag{26}$$

where

$$\begin{aligned}
\eta_{1,x} &= \upsilon_{1,x,t}-f''_{2,x,t}+w_2\upsilon_{2,x,t}+w_0 f,\\
\eta_{1,y} &= \upsilon_{1,y,t}-f''_{2,y,t}+w_2\upsilon_{2,y,t},\\
\eta_{2,x} &= \upsilon_{2,x,t}+f''_{2,x,t}+w_2\upsilon_{1,x,t}+w_0 f,\\
\eta_{2,y} &= \upsilon_{2,y,t}+f''_{2,y,t}+w_2\upsilon_{1,y,t}.
\end{aligned} \tag{27}$$

The *Jacobian matrix* $\mathbf{J}$ of Eq. (26) can be obtained, i.e.,

$$\begin{aligned}
J_{1,1} &= \frac{\upsilon_{max}}{\varphi_3}-\frac{2\upsilon_{max}\varphi_2^2}{2\varphi_4} & J_{1,2} &= -\frac{2\upsilon_{max}\varphi_1\varphi_2}{2\varphi_4}\\
J_{1,3} &= \frac{w_2\upsilon_{max}}{\varphi_3}-\frac{w_2\upsilon_{max}\varphi_2^2}{\varphi_4} & J_{1,4} &= -\frac{w_2\upsilon_{max}\varphi_1\varphi_2}{\varphi_4}\\
J_{1,5} &= \frac{2\upsilon_{max}\varphi_2^2}{2\varphi_4}-\frac{\upsilon_{max}}{\varphi_3} & J_{1,6} &= \frac{2\upsilon_{max}\varphi_1\varphi_2}{2\varphi_4}
\end{aligned} \tag{28}$$

$$\begin{aligned}
J_{2,1} &= -\frac{2\upsilon_{max}\varphi_1\varphi_2}{2\varphi_4} & J_{2,2} &= \frac{\upsilon_{max}}{\varphi_3}-\frac{2\upsilon_{max}\varphi_1^2}{2\varphi_4}\\
J_{2,3} &= -\frac{\upsilon_{max}w_2\varphi_1\varphi_2}{\varphi_4} & J_{2,4} &= \frac{\upsilon_{max}w_2}{\varphi_3}-\frac{\upsilon_{max}w_2\varphi_1^2}{\varphi_4}\\
J_{2,5} &= \frac{2\upsilon_{max}\varphi_1\varphi_2}{2\varphi_4} & J_{2,6} &= \frac{2\upsilon_{max}\varphi_1^2}{2\varphi_4}-\frac{vmax}{\varphi_3}
\end{aligned} \tag{29}$$

$$\begin{aligned}
J_{3,1} &= \frac{\upsilon_{max}w_2}{\psi_3}-\frac{\upsilon_{max}w_2\psi_1^2}{\psi_4} & J_{3,2} &= -\frac{\upsilon_{max}w_2\psi_1\psi_2}{\psi_4}\\
J_{3,3} &= \frac{\upsilon_{max}}{\psi_3}-\frac{2\upsilon_{max}\psi_1^2}{2\psi_4} & J_{3,4} &= -\frac{2\upsilon_{max}\psi_1\psi_2}{2\psi_4}\\
J_{3,5} &= \frac{\upsilon_{max}}{\psi_3}-\frac{2\upsilon_{max}\psi_1^2}{2\psi_4} & J_{3,6} &= -\frac{2\upsilon_{max}\psi_1\psi_2}{2\psi_4}
\end{aligned} \tag{30}$$

$$J_{4,1} = -\frac{\upsilon_{max} w_2 \psi_1 \psi_2}{\psi_4} \quad J_{4,2} = \frac{\upsilon_{max} w_2}{\psi_3} - \frac{\upsilon_{max} w_2 \psi_2^2}{\psi_4}$$
$$J_{4,3} = -\frac{2\upsilon_{max} \psi_1 \psi_2}{2\psi_4} \quad J_{4,4} = \frac{\upsilon_{max}}{\psi_3} - \frac{2\upsilon_{max} \psi_2^2}{2\psi_4} \tag{31}$$
$$J_{4,5} = -\frac{2\upsilon_{max} \psi_1 \psi_2}{2\psi_4} \quad J_{4,6} = \frac{\upsilon_{max}}{\psi_3} - \frac{2\upsilon_{max} \psi_2^2}{2\psi_4}$$

$$J_{5,1} = 2w_1 \quad J_{5,2} = 0 \quad J_{5,3} = -2w_1$$
$$J_{5,4} = 0 \quad J_{5,5} = 1 \quad J_{5,6} = 0 \tag{32}$$

$$J_{6,1} = 0 \quad J_{6,2} = 2w_1 \quad J_{6,3} = 0$$
$$J_{6,4} = -2w_1 \quad J_{6,5} = 0 \quad J_{6,6} = 1 \tag{33}$$

where

$$\begin{aligned}
\varphi_1 &= \upsilon_{1,y} - f''_{2,x} + w_2 \upsilon_{2,y} \\
\varphi_2 &= w_0 f - f''_{2,x} + \upsilon_{1,x} + w_2 \upsilon_{2,x} \\
\varphi_3 &= \sqrt{\varphi_1^2 + \varphi_2^2} \\
\varphi_4 &= (\varphi_1^2 + \varphi_2^2)^{\frac{3}{2}} \\
\psi_1 &= w_0 f + f''_{2,x} + \upsilon_{2,x} + w_2 \upsilon_{1,x} \\
\psi_2 &= f''_{2,y} + \upsilon_{2,y} + w_2 \upsilon_{1,y} \\
\psi_3 &= \sqrt{\psi_1^2 + \psi_2^2} \\
\psi_4 &= (\psi_1^2 + \psi_2^2)^{\frac{3}{2}}.
\end{aligned} \tag{34}$$

The *Jacobian matrix* corresponding to the Formation 1 is

$$\mathbf{J} = \begin{pmatrix} 0 & 0 & 0 & 0 & 0 & 0 \\ 0 & 0.1653 & 0 & 0.8264 & 0 & -0.1653 \\ 0 & 0 & 0 & 0 & 0 & 0 \\ 0 & 0.8264 & 0 & 0.1653 & 0 & 0.1653 \\ 1 & 0 & -1 & 0 & 1 & 0 \\ 0 & 1 & 0 & -1 & 0 & 1 \end{pmatrix}. \tag{35}$$

One can obtain the corresponding eigenvalues, i.e.,

$$\lambda_1 = 1 \quad \lambda_2 = 0 \quad \lambda_3 = 0$$
$$\lambda_4 = -0.4300 \quad \lambda_5 = 0.9917 \quad \lambda_6 = 0.7688 \quad . \tag{36}$$

The absolute values of each eigenvalue is not greater than 1, i.e.,

$$|\lambda_j| \leqslant 1, \quad (j = 1,2,3,4,5,6), \tag{37}$$

consequently, the flight formation corresponding to the Formation 1 is stable. The *Jacobian matrix* of the Formation 2 is

$$\mathbf{J} = \begin{pmatrix} 0 & 0 & 0 & 0 & 0 & 0 \\ 0 & 0.1681 & 0 & 0.8403 & 0 & -0.1681 \\ 0 & 0 & 0 & 0 & 0 & 0 \\ 0 & 0.8403 & 0 & 0.1681 & 0 & 0.1681 \\ 1 & 0 & -1 & 0 & 1 & 0 \\ 0 & 1 & 0 & -1 & 0 & 1 \end{pmatrix}. \tag{38}$$

The corresponding eigenvalues is

$$\begin{array}{lll} \lambda_1 = 1 & \lambda_2 = 0 & \lambda_3 = 0 \\ \lambda_4 = -0.4386 & \lambda_5 = 1.0084 & \lambda_6 = 0.7663 \quad . \end{array} \tag{39}$$

Because the absolute value of eigenvalue λ_5 is greater than 1, the flight formation corresponding to Formation 2 is unstable.

In the same way, one can obtain that the flight formation corresponding to Formation 3 is stable, while the flight formation corresponding to Formation 4 is unstable.

When there are a large number of individuals, even if the flight direction of the flock is not the direction of the migration force, the attractive force, repulsive force and migration force among individuals may reach a balance, i.e., $w_1\vec{F}_i' + w_3\vec{F}_i''' + w_0\vec{f} = 0$, so that the formation can fly in any direction. This type of flight formations is called Formation 1-like solutions. For instance, the flight formations in Fig. 1A and 1B are Formation 1-like solutions. In these two formations, the relative positions of individuals remain unchanged, which also indicates that the migration force, the attractive force, repulsive force and migration force among individuals have reached a balance. Note that, in the flight formation in Fig. 1B, Although the flight direction of the formation is constantly changing, the flight directions of all individuals remain highly consistent. That is, the flock have a high polarization intensity (see Fig. 2A). Therefore, the relative position between individuals can be maintained. Because the initial conditions of formations are the random distributions of individuals in a rectangular space, it is easier for birds to enter Formation 1-like solution.

Form Eq. (17), the conditions for the existence of Formations 1 and 2 can be obtained, i.e.,

$$w_3 \leqslant w_1 r_2^2 = 0.045. \tag{40}$$

This means that when w_3 is less than or equal to 0.045, Formations 1 and 2 exist, and when w_3 is greater than 0.045, Formations 1 and 2 do not exist. Accordingly, when w_3 is greater than 0.045, the flock can only be stable in the Formation 3 (see Fig. 1D). Note that the flight formation in Fig. 1C is a critical phenomenon, changing back and forth between the two formations (Formation 1-like and Formation 3 solutions).

5. Conclusion and Discussion

In this article, we applied the modified Biod model to migrating bird flocks. Based on this improved model, we tested the effect of the weight of repulsion force between individuals on flight formations. As the weight of repulsive force between individuals is gradually increased, a phase transition of the flight formation is observed. This phase transition could explain the differences in flight formations between small and large birds. In summary, we have studied the formation mechanisms of flight formations of migrating bird flocks from a new perspective. The results show that differences in the weight of repulsive forces between individuals cause different flight formations. Larger weight of repulsive forces leads to more orderly flight formations, while smaller weight of repulsive forces leads to more disorderly flight formations. Compared with the energy-saving hypothesis and visual communication hypothesis, our findings not only explain the formation mechanisms of flight formations of large birds, but also explain the differences between flight formations of large and small birds. In addition, we also studied the effects of the total number and average density of individuals on flight formations of large bird flocks, and obtained three types of states of the flight formations. Larger numbers or average density may cause flight formations to lose the ability to migrate.

In the face of the actual task and the sudden change of the environment, the ability to select the optimal formation and carry out formation transformation as quickly as possible is an effective evaluation index of the formation control technology of UAV swarms [27, 30, 31, 32, 33]. Reference [32] studies the formation transformation and formation keeping. First, the control method of proportional integration and differentiation is adopted to ensure that the UAVs can form a special formation, and then the formation transformation is realized by adjusting the formation spacing, which realizes the dynamic formation transformation of UAV swarms. Lin et al. introduced Laplacian operator to discuss formation coordination problem and used proxy network to realize the transformation of a specific formation [33]. Giacomin et al. studied the formation transformation of UAVs and designed a distributed algorithm based on trajectory segmentation. Specially, aiming at the conversion of UAV's linear formation to circular formation, the fast formation transformation of UAVs is realized by using the real-time track planning algorithm of trajectory segmentation

calculation [34]. However, when the number of individuals is too large, the efficiency of the above method will be greatly reduced. Therefore, there is still a need to develop new methods to control the formation transformation of swarms containing a large number of individuals. In this article, through numerical simulation, we realize the transformation of a swarm containing a large number of individuals from a triangular formation to a linear formation. Our future work will focus on applying this approach to the formation control of actual UAVs.

Acknowledgements

This work is supported by the National Natural Science Foundation of China under Grant Nos. 11875042 (C. Gu) and 11505114 (C. Gu), and the Shanghai project for construction of top disciplines under Grant No. USST-SYS01 (H. Yang and C. Gu).

Supplementary materials

Movie S1. Migration formations of large birds.
Movie S2 and S3. Evolution of the formation of the bird flocks when w_3 is equal to 0.01 with $N = 20$ and $\rho = 5$. The horizon in this Movie is 4×4.
Movie S4. Evolution of the formation of the bird flocks when w_3 is equal to 0.02 with $N = 20$ and $\rho = 5$. The horizon in this Movie is 4×4.
Movie S5. Evolution of the formation of the bird flocks when w_3 is equal to 0.05 with $N = 20$ and $\rho = 5$. The horizon in this Movie is 12×12.
Movie S6. Evolution of the formation of the bird flocks when w_3 is equal to 0.10 with $N = 20$ and $\rho = 5$. The horizon in this Movie is 12×12.
Movie S7. Evolution of the formation of the bird flocks when w_3 is equal to 0.30 with $N = 20$ and $\rho = 5$. The horizon in this Movie is 12×12.
Movie S8. Evolution of the formation of the bird flocks when w_3 is equal to 0.35 with $N = 20$ and $\rho = 5$. The horizon in this Movie is 12×12.
Movie S9. The collective behaviour exhibited by the model when N is equal to 100 with $w_3 = 1.25$ and $\rho = 5$. The horizon in this Movie is 40×40.
Movie S10. The collective behaviour exhibited by the model when N is equal to 120 with $w_3 = 1.25$ and $\rho = 5$. The horizon in this Movie is 60×60.
Movie S11. The collective behaviour exhibited by the model when N is equal to 150 with $w_3 = 1.25$ and $\rho = 5$. The horizon in this Movie is 10×10.
Movie S12. The collective behaviour exhibited by the model when ρ is equal to 0.1 with $w_3 = 1.25$ and $N = 300$. The horizon in this Movie is 80×80.
Movie S13. The collective behaviour exhibited by the model when ρ is equal to 1 with $w_3 = 1.25$ and $N = 300$. The horizon in this Movie is 80×80.
Movie S14. The collective behaviour exhibited by the model when ρ is equal to 3 with $w_3 = 1.25$ and $N = 300$. The horizon in this Movie is 80×80.

References

[1] M. Andersson. Kin selection and reciprocity in flight formation. Behavioral Ecology **15**, 158-162 (2004).
[2] T. Alerstam. Bird migration. Cambridge: Cambridge University Press 1990.
[3] A. Cavagna, A. Cimarelli, I. Giardina, et al. Scale-free correlations in starling flocks. PNAS 107, 11865-11870 (2010).
[4] D. J. G. Pearce, A. M. Miller, G. Rowlands, et al. Role of projection in the control of bird flocks. Proceedings of the National Academy of Sciences **111**, 10422-10426 (2014).
[5] J. R. Speakman, D. Banks. The function of flight formations in Greylag Geese Anser anser; energy saving or orientation. Ibis **140**, 280-287 (2008).
[6] C. J. Cutts, J. R. Speakman. Energy savings in formation flight of Pink-footed Geese. Journal of Experimental Biology **189**, 251-261 (1994).
[7] I. L. Bajec, F. H. Heppner. Organized flight in birds. Animal Behaviour **78**, 777-789 (2009).
[8] P. B. S Lissaman, C. A. Shollenberger. Formation Flight of Birds. Science **168**, 1003-1005 (1970).
[9] J. P. Badgerow. An analysis of function in the formation flight of Canada geese. Auk **105**, 749-755 (1988).
[10] F. R. Hainsworth. Precision and Dynamics of Positioning by Canada Geese Flying in Formation. Journal of Experimental Biology **128**, 445-462 (1987).
[11] P. Seiler, A. Pant, K. Hedrick. Analysis of bird formations, IEEE Conference on Decision & Control. IEEE (2002).
[12] D. Hummel. Formation flight as an energy-saving mechanism. Israel Journal of Zoology **41**, 261-278 (2013).
[13] H. Weimerskirch, J. Martin, Y. Clerquin, et al. Energy saving in flight formation. Nature **413**, 697-698 (2001).
[14] I. D. Couzin, J. Krause. Self-organization and collective behavior in vertebrates. Adv Stud Behav **32**, 1-75 (2003).
[15] C. W. Reynolds. Flocks, herds and schools: A distributed behavioral model. Comput Graph **21**, 25-34 (1987).
[16] S. Gueron, S. A. Levin. Rubenstein DI The dynamics of herds: From individuals to aggregations. J Theor Biol **182**, 85-98 (1996).
[17] T. Vicsek, A. Czirok, E. BenJacob, I. Cohen, O. Shochet. Novel type of phase-transition in a system of self-driven particles. Phys Rev Lett. **75**, 1226-1229 (1995).
[18] G. Gregoire, H. Chate. Onset of collective and cohesive motion. Phys Rev Lett. **92**, 025702 (2004).
[19] H. Chate, F. Ginelli, G. Gregoire, F. Raynaud. Collective motion of self-propelled particles interacting without cohesion. Phys Rev E **77**, 046113 (2008).
[20] H. P. Zhang, A. Be'er, E. L. Florin, et al. Collective motion and density fluctuations in bacterial colonies. PNAS **107**, 13626-13630 (2010).
[21] A. Gelblum, I. Pinkoviezky, E. Fonio, et al. Emergent oscillations assist obstacle negotiation during ant cooperative transport. Proceedings of the National Academy of Sciences **113**, 14615-14620 (2016).
[22] A. Cavagna, L. Del Castello, I. Giardina, et al. Flocking and Turning: a New Model for Self-organized Collective Motion. Journal of Statistical Physics **158**, 601-627 (2015).

[23] M. Moussaid, D. Helbing, G. Theraulaz. How simple rules determine pedestrian behavior and crowd disasters. Proceedings of the National Academy of Sciences **108**, 6884-6888 (2011).
[24] J. Li, L. Jingyu, S. Chao, et al. Obstacle Optimization for Panic Flow-Reducing the Tangential Momentum Increases the Escape Speed. PLoS ONE **9**, e115463 (2014).
[25] D. Helbing, I. J. Farkas, T. Vicsek. Simulating Dynamical Features of Escape Panic. Social Science Electronic Publishing **407**, 487-90 (2000).
[26] H. Duan, H. Qiu. Unmanned Aerial Vehicle Distributed Formation Rotation Control Inspired by Leader-Follower Reciprocation of Migrant Birds. IEEE Access **99**, 1-1 (2018).
[27] H. Duan, H. Qiu. Unmanned aerial vehicle swarm autonomous control based on swarm intelligence. Beijing: Science Press, 2018.
[28] S. Hauert, S. Leven, M. Varga, et al. Reynolds flocking in reality with fixed-wing robots: communication range vs. maximum turning rate. IEEE/RSJ International Conference on Intelligent Robots & Systems. IEEE, 5015-5020 (2011).
[29] L. Shen. Theory and Technology of autonomous control of mobile robot. Beijing: Science Press, 2011.
[30] L. Shen, T. Niu, H. Zhu. Theories and methods of autonomous cooperative control for multiple UAVs. Beijing: National Defense Industry Press, 2018.
[31] Y. Wang, C. Huang, L. He. Adaptive time-varying formation tracking control of unmanned aerial vehicles with quantized input. ISA Transactions **85**, 76-83 (2018).
[32] D. Luo, W. Xu, S. Wu, et al. UAV formation flight control and formation switch strategy. International Conference on Computer Science & Education. IEEE **8**, 264-269 (2013).
[33] Z. Lin, L. Wang, Z. Han, et al. Distributed Formation Control of Multi-Agent Systems Using Complex Laplacian. IEEE Transactions on Automatic Control **59**, 1765-1777 (2014).
[34] P. A. Giacomin, E. M. Hemerly. Reconfiguration Between Longitudinal and Circular Formations for Multi-UAV Systems by Using Segments. Journal of Intelligent & Robotic Systems **78**, 1-17 (2014).
[35] I. D. Couzin, J. Krause, R. James, et al. Collective Memory and Spatial Sorting in Animal Groups. Journal of Theoretical Biology **218**, 1-11 (2002).

Declaration of Interest Statement

The authors declare that they have no conflict of interest, and this manuscript is approved by all authors for publication. I would like to declare on behalf of my co-authors that the work described was original research that has not been published previously, and not under consideration for publication elsewhere, in whole or in part. All the authors listed have approved the manuscript.

Credit Author Statement

Use this form to specify the contribution of each author of your manuscript. A distinction is made between five types of contributions: Conceived and designed the analysis; Collected the dada; Contribution data or analysis tools; Performed the analysis; Wrote the paper.

For each author of your manuscript, please indicate the types of contributions the author has made. An author may have made more than one type of contribution. Optionally, for each contribution type, you may specify the contribution of an author in more detail by providing a one-sentence statement in which the contribution for instance could be specified in more detail as 'Performed the computer simulations', 'Performed the statistical analysis', or 'Performed the text mining analysis'.
If an author has made a contribution that is not covered by the five pre-defined contribution types, then please choose 'Other contribution' and provide a one-sentence statement summarizing the author's contribution.

Manuscript title: A type of bi-stable spiral wave in a single-period oscillatory medium

Author 1: Jian Gao

- ☑ **Conceived and designed the analysis**
  Specify contribution in more detail(optional; no more than one sentence)
- ☑ **Collected the data**
  Specify contribution in more detail(optional; no more than one sentence)
- ☑ **Contributed data or analysis tools**
  Specify contribution in more detail(optional; no more than one sentence)
- ☑ **Performed the analysis**
  Specify contribution in more detail(optional; no more than one sentence)
- ☑ **Wrote the paper**
  Specify contribution in more detail(optional; no more than one sentence)
- ☐ **Other contribution**
  Specify contribution in more detail(optional; no more than one sentence)

Author 2: Changgui Gu

- ☐ **Conceived and designed the analysis**
  Specify contribution in more detail(optional; no more than one sentence)
- ☐ **Collected the data**
  Specify contribution in more detail(optional; no more than one sentence)
- ☑ **Contributed data or analysis tools**
  Specify contribution in more detail(optional; no more than one sentence)

☑ **Performed the analysis**

Specify contribution in more detail(optional; no more than one sentence)

☑ **Wrote the paper**

Specify contribution in more detail(optional; no more than one sentence)

☐ **Other contribution**

Specify contribution in more detail(optional; no more than one sentence)

Author 3: Huijie Yang

☐ **Conceived and designed the analysis**

Specify contribution in more detail(optional; no more than one sentence)

☐ **Collected the data**

Specify contribution in more detail(optional; no more than one sentence)

☐ **Contributed data or analysis tools**

Specify contribution in more detail(optional; no more than one sentence)

☑ **Performed the analysis**

Specify contribution in more detail(optional; no more than one sentence)

☐ **Wrote the paper**

Specify contribution in more detail(optional; no more than one sentence)

☐ **Other contribution**

Specify contribution in more detail(optional; no more than one sentence)

Author 4: Man Wang

☐ **Conceived and designed the analysis**

Specify contribution in more detail(optional; no more than one sentence)

☐ **Collected the data**

Specify contribution in more detail(optional; no more than one sentence)

☐ **Contributed data or analysis tools**

Specify contribution in more detail(optional; no more than one sentence)

☐ **Performed the analysis**

Specify contribution in more detail(optional; no more than one sentence)

☑ **Wrote the paper**

Specify contribution in more detail(optional; no more than one sentence)

☑ **Other contribution**

Specify contribution in more detail(optional; no more than one sentence)